

Figure S1. 3D representation of redocking of crystallographic structures of the WT-FLT3 model (DFG-out and DFG-in) and its co-crystallized ligands. (A) 6IL3 structure with A9R. (B) WT-FLT3/DFG-out structure with A9R. (C) 1PKG structure with ADP. (D) WT-FLT3/DFG-in structure with ADP (images obtained using PyMOL v. 2.5.4). The light pink color represents the crystallographic structures with their ligand inhibitors (light blue) and the purple color represents redocking with the ligand inhibitors (blue). A9R, 7-methoxy-6-(1-methyl-1H-pyrazol-4-yl)-3-(pyridin-2-yl)imidazo[1,2-a]pyridine; ADP, adenosine diphosphate; DFG-in, active aspartic acid-phenylalanine-glycine motif; DFG-out, inactive aspartic acid-phenylalanine-glycine motif; FLT3, FMS-like tyrosine kinase 3; WT, wild-type.

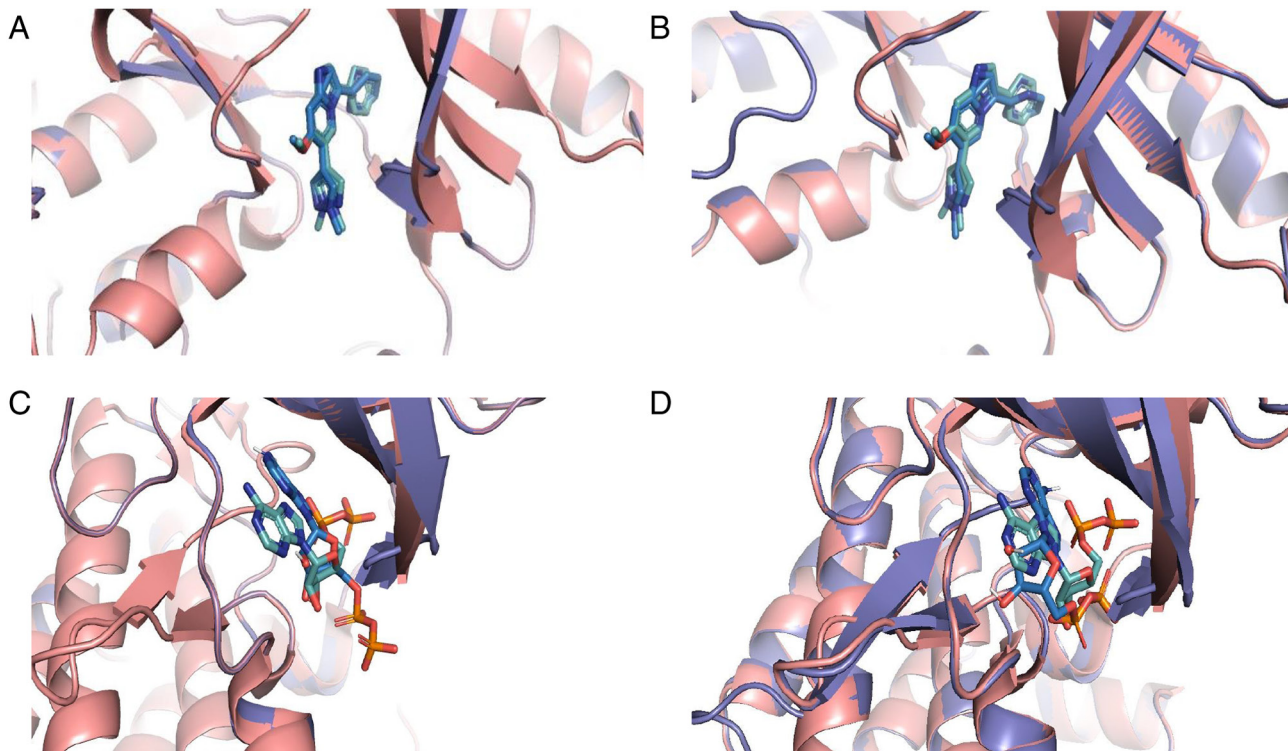


Figure S3. ERRAT plots of the FLT3 models. (A) ERRAT plot and score of WT-FLT3/DFG-out. (B) ERRAT plot and score of WT-FLT3/DFG-in. (C) ERRAT plot and score of ITD-FLT3/DFG-out. (D) ERRAT plot and score of ITD-FLT3/DFG-in. Red bars indicate the misfolded regions, yellow bars indicate the error regions (error values falling in the 95-99% range) and white bars indicate lower error regions for protein folding. *Error axis, two lines are drawn to indicate the confidence with which it is possible to reject regions that exceed that error value. DFG-in, active aspartic acid-phenylalanine-glycine motif; DFG-out, inactive aspartic acid-phenylalanine-glycine motif; FLT3, FMS-like tyrosine kinase 3; ITD, internal tandem duplication; WT, wild-type.

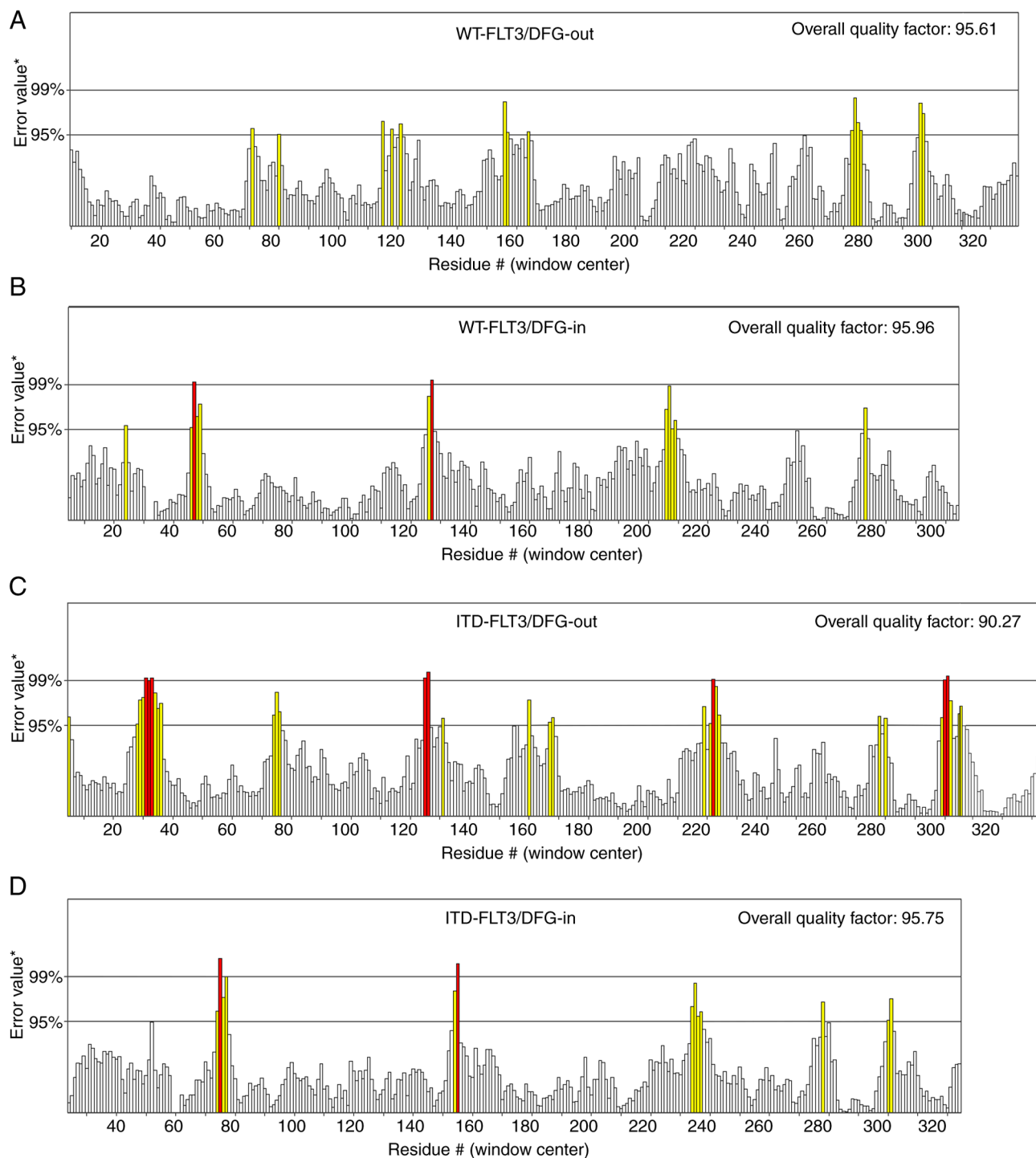


Figure S4. Flow cytometric analysis of FLT3 expression in MV4-11 and HL60 cells, and PBMCs. Dot plots of acute myeloid leukemic cell lines and PBMC populations, and histograms showing staining with anti-FLT3 antibody and isotype control antibody. Data are presented as mean fluorescence indexes. (A) MV4-11 cells. (B) HL60 cells. (C) PBMCs. FLT3, FMS-like tyrosine kinase 3; FSC-A, forward scatter area; FSC-H, forward scatter height; PBMCs, peripheral blood mononuclear cells; SSC-A, side scatter area.

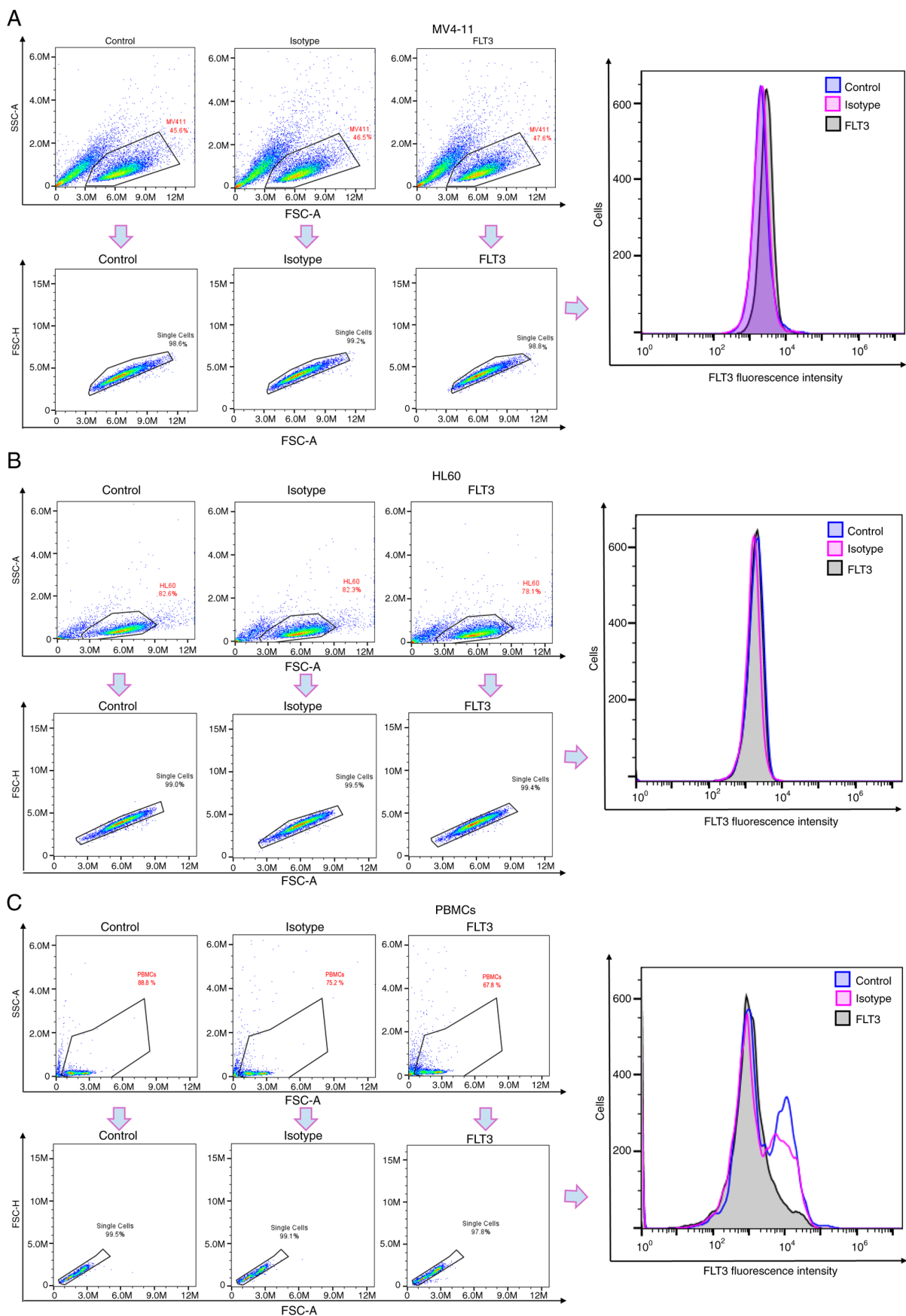


Figure S5. Dot plot representation of the effect of gilteritinib and quizartinib on the induction of apoptosis in acute myeloid leukemiacell lines and PBMCs. Cells were stained with annexin V-FITC and PI. Control -, no treatment; death control, 3% DMSO; etoposide, 100 nM etoposide. PBMCs, peripheral blood mononuclear cells.

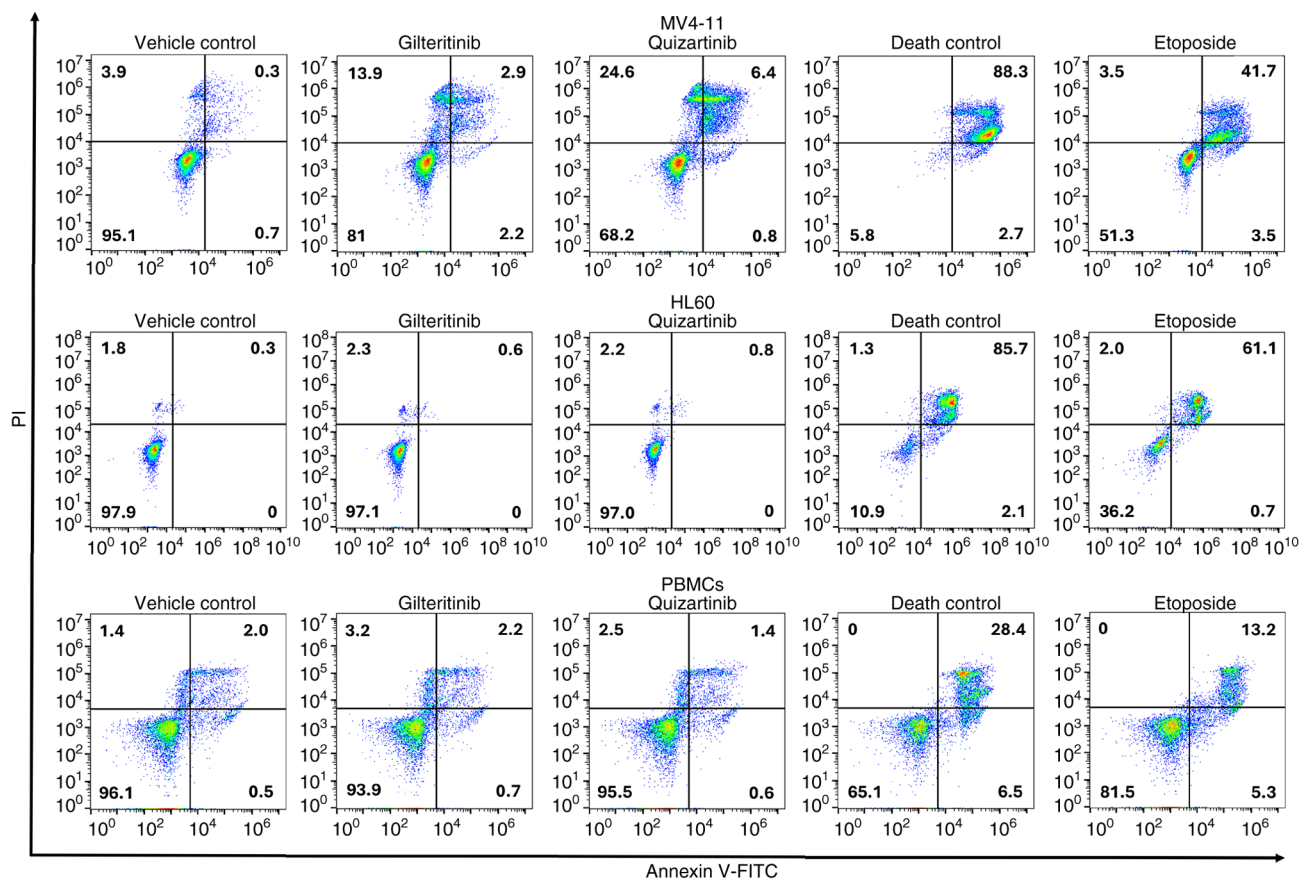


Figure S6. Flow cytometry analysis of MV4-11 cell division using CFSE. MV4-11 cells were exposed to gilteritinib, quizartinib and control conditions. (A) Analysis strategy. (B) No treatment (0 nM; 0 h). (C) No treatment (0 nM; 48 h). (D) Vehicle control (0.1% DMSO). (E) Gilteritinib (7.99 nM). (F) Quizartinib (4.76 nM). (G) Death control (3% DMSO). (H) Etoposide (100 nM). CFSE, carboxyfluorescein succinimidyl ester; FSC-A, forward scatter area; FSC-H, forward scatter height; SSC-A, side scatter area.

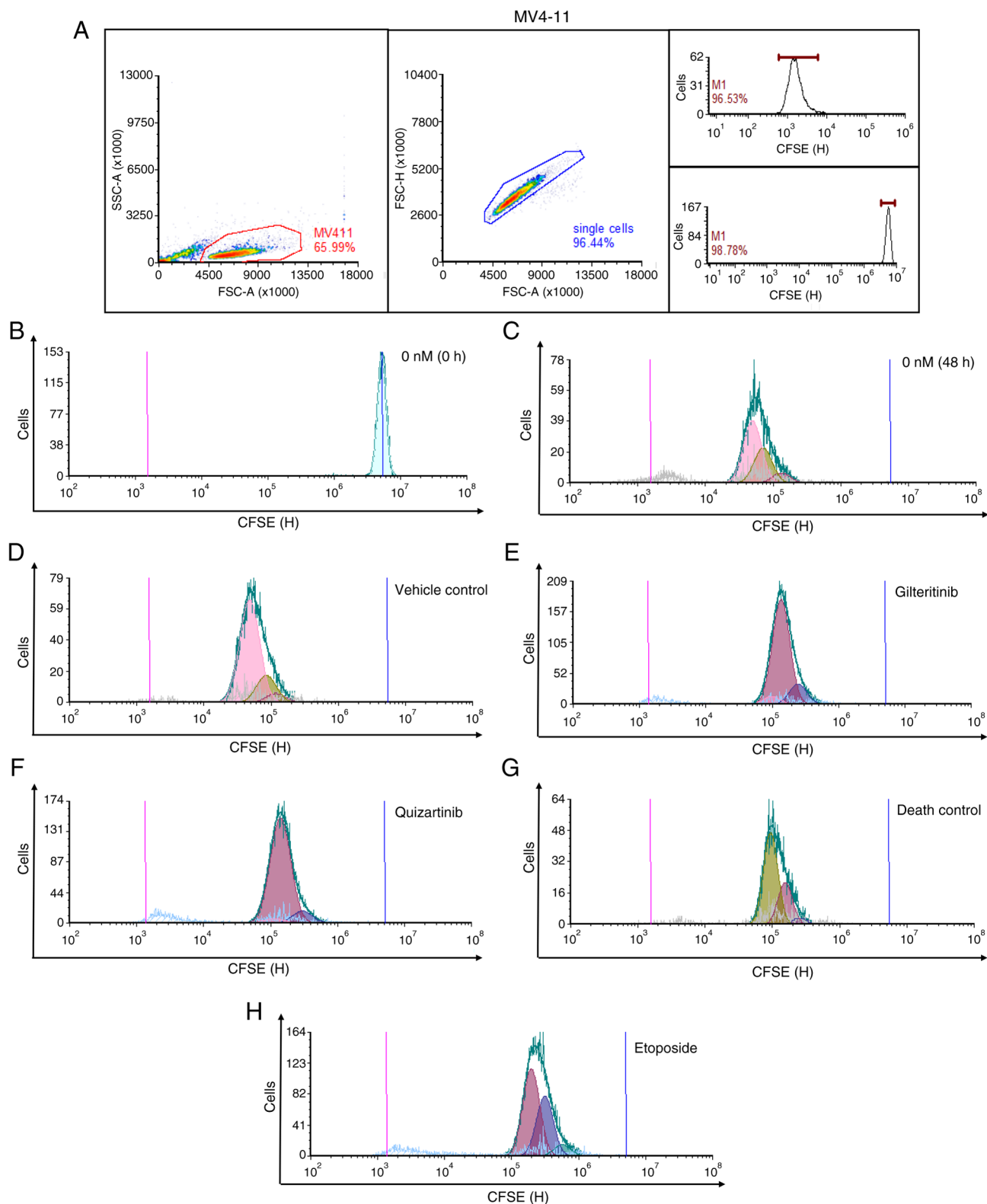


Figure S7. Flow cytometry analysis of HL60 cell division using CFSE. HL60 cells were exposed to gilteritinib, quizartinib and control conditions. (A) Analysis strategy. (B) No treatment (0 nM; 0 h). (C) No treatment (0 nM; 48 h). (D) Vehicle control (0.1% DMSO). (E) Gilteritinib (7.99 nM). (F) Quizartinib (4.76 nM). (G) Death control (3% DMSO). (H) Etoposide (100 nM). CFSE, carboxyfluorescein succinimidyl ester; FSC-A, forward scatter area; FSC-H, forward scatter height; SSC-A, side scatter area.

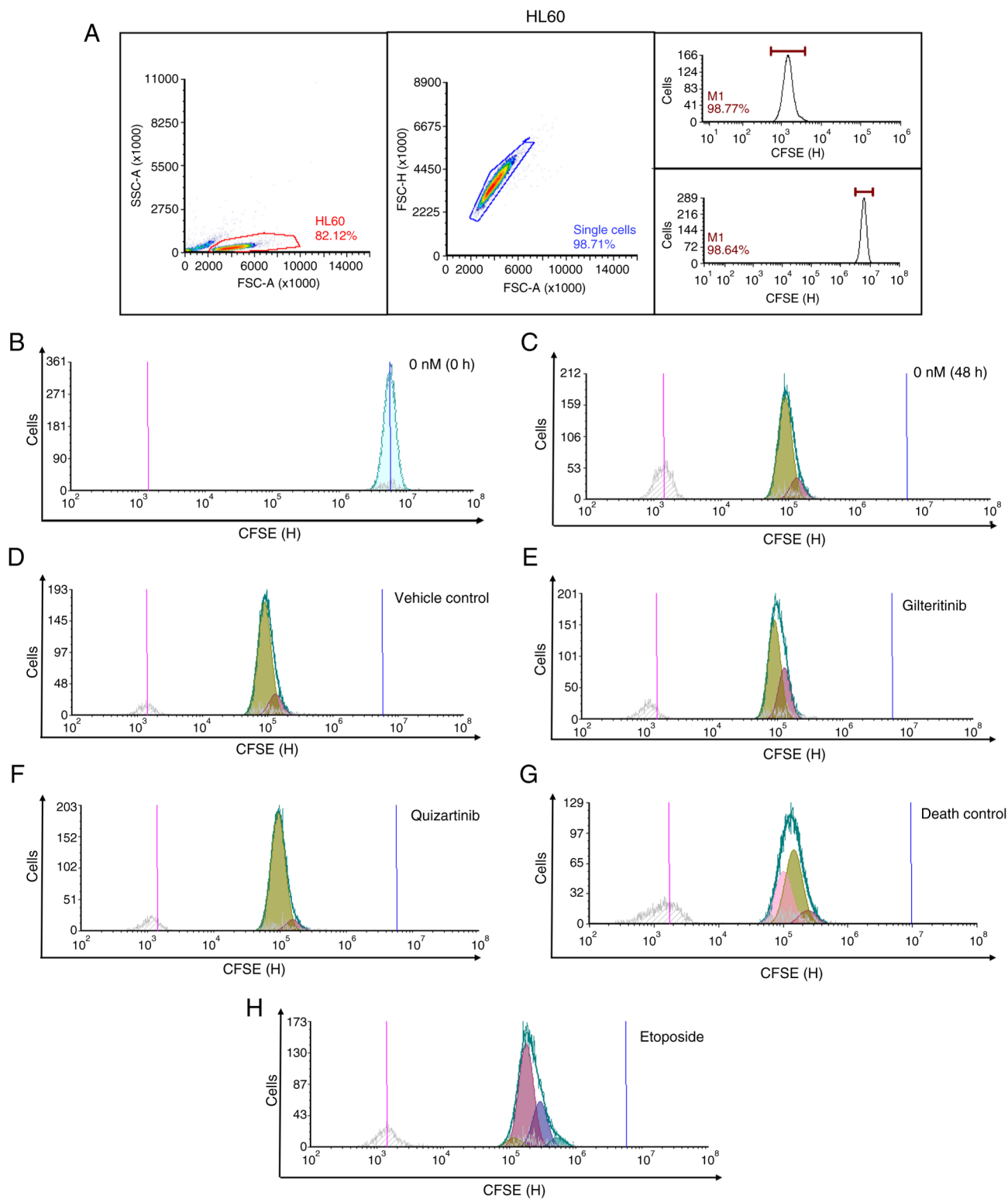


Figure S8. Flow cytometry analysis of PBMC division using CFSE. PBMCs were exposed to gilteritinib, quizartinib and control conditions. (A) Analysis strategy. (B) No treatment (0 nM; 0 h). (C) No treatment (0 nM; 48 h). (D) Vehicle control (0.1% DMSO). (E) Gilteritinib (7.99 nM). (F) Quizartinib (4.76 nM). (G) Death control (3% DMSO). (H) Etoposide (100 nM). CFSE, carboxyfluorescein succinimidyl ester; FSC-A, forward scatter area; FSC-H, forward scatter height; PBMCs, peripheral blood mononuclear cells; SSC-A, side scatter area.

